 

*ACTIVE MEDIA*

PACS numbers: 42.55.Rz; 42.70.Hj
DOI: 10.1070/QE2011v041n11ABEH14575

# Laser and thermal characteristics of Yb:YAG crystals in the 80–300 K temperature range

I.B. Mukhin, O.V. Palashov, E.A. Khazanov, A.G. Vyatkin, E.A. Perevezentsev

*Abstract.* **The spectral and thermooptical characteristics of an Yb:YAG crystal were measured in the 80–300 K temperature range. On cooling the crystal, the amplification cross section increases fivefold, the peak of the cross section spectrum shifts from 1030.1 to 1029.3 nm, and its width lowers from ~10 to 1.3 nm. These effects must be taken into account when operating with cryogenic amplifiers. Also measured were thermooptical constants *P* and *Q* as well as the photoelastic anisotropy parameter. These material constants completely determine the thermal and phase polarisation distortions in an active element when the heat release and the thermal conductivity coefficient are known. The thermoinduced depolarisation was shown to lower by a factor of 1000 and the optical strength by a factor of 50 on cooling the Yb:YAG crystal to a temperature of 78 K.**

***Keywords:*** *amplification cross section, thermoinduced distortions, Yb:YAG, cryogenic temperatures.*

## 1. Introduction

Ytterbium (Yb) ion doped laser media are used increasingly to make lasers with high average and peak powers. This is primarily due to the emergence of high-efficiency diode lasers producing radiation at wavelengths $\lambda = 900-100$ nm, i.e., in the spectral domain containing Yb-ion absorption peaks. It is seen that the Yb ion offers several advantages over the neodymium (Nd) ion from the standpoint of their laser properties. The ytterbium ion is characterised by a small quantum defect (~9%) and the absence of absorption from its excited state [1, 2]. The relatively long lifetime of its state permits, despite the low peak power of diode pumping, storing an energy comparable to the energy stored in excited Nd ions under flashlamp pumping. Owing to heavy doping, disk Yb-ion lasers may exhibit a high efficiency for a high average output power. Heat removal from the disk face furnishes an opportunity to efficiently solve the cooling problem, and a high Yb-ion density provides a high gain [3]. Due to a low disk thickness it is possible to rule out the effect of radiation self-focusing in pulsed lasers with a high peak power.

On the other hand, the Yb ion has several disadvantages. The energies of the ground level and the lower laser level are little different in the Yb ion. That is why approximately 5% of the total number of ions are in the lower laser level of Yb at room temperature (according to the Boltzmann distribution). The system of laser levels similar to that of the Yb ion is referred to as a quasi-four-level system. Another significant disadvantage of the Yb ion is its small amplification cross section. In this connection, cooling the active medium of Yb:YAG lasers to cryogenic temperatures (80–200 K) holds much promise. On cooling, the lower laser level is depleted, the laser medium becomes a four-level one, the amplification and absorption cross sections increase [4, 5], as does the thermal conductivity coefficient. In this case, polarisation and phase distortions arising from variations of the optical crystal characteristics become substantially smaller [6–8], making it possible to increase the thermal load on the active element.

The idea of making an Yb:YAG laser operating at liquid nitrogen temperatures was proposed and realised in Refs [9, 10]. In Refs [11, 12] it was shown that this laser may possess a high efficiency and exhibit an excellent beam quality. Despite the urgency of developing cryogenic Yb:YAG lasers, the temperature dependences of Yb:YAG crystal characteristics have not been adequately studied. There is a discordance between the data of several papers.

In this work we generalise the data available from the literature and also give the data of our measurements of the laser and thermal Yb:YAG crystal characteristics in the 80–300 K temperature range.

## 2. Spectral characteristics

One of the main Yb:YAG characteristics – the amplification cross section – has been adequately investigated at room temperature [13–15]. In Ref. [11] it is stated that the amplification cross section increases approximately seven-fold on cooling the Yb:YAG crystal to 77 K; also given are luminescence spectra at 77, 150, and 300 K [11]. The temperature dependences of the spectrum width, the peak amplification cross section, and the lifetime of the Yb excited state were investigated for different degrees of doping [7].

In our work the spectrum of amplification cross section was studied in greater detail. The experimental arrangement is schematised in Fig. 1a. A 0.3-mm thick Yb:YAG crystal with an ytterbium ion density of 10% was brazed to a copper plate placed in a cryostat. The cryostat was a vacuum chamber with a liquid nitrogen-cooled vessel, which was in direct thermal contact with the specimen under investigation. The cooling of the copper plate was monitored with a calibrated thermal sensor. The $\lambda \sim 938$ nm pump radiation was directed onto the crystal through an optical window. Absorption at this wavelength in Yb:YAG is temperature-independent [5]. The absorbed pump power $P_{abs}$ did not exceed 10 W for a 3-mm beam diameter on

**I.B. Mukhin, O.V. Palashov, E.A. Khazanov, A.G. Vyatkin, E.A. Perevezentsev** Institute of Applied Physics, Russian Academy of Sciences, ul. Ul'yanova, 46, 603950 Nizhnii Novgorod, Russia; e-mail: mib1982@mail.ru

Received 27 February 2011, revised 22 August 2011.
*Kvantovaya Elektronika* **41** (11) 1045–1050 (2011)
Translated by E.N. Ragozin

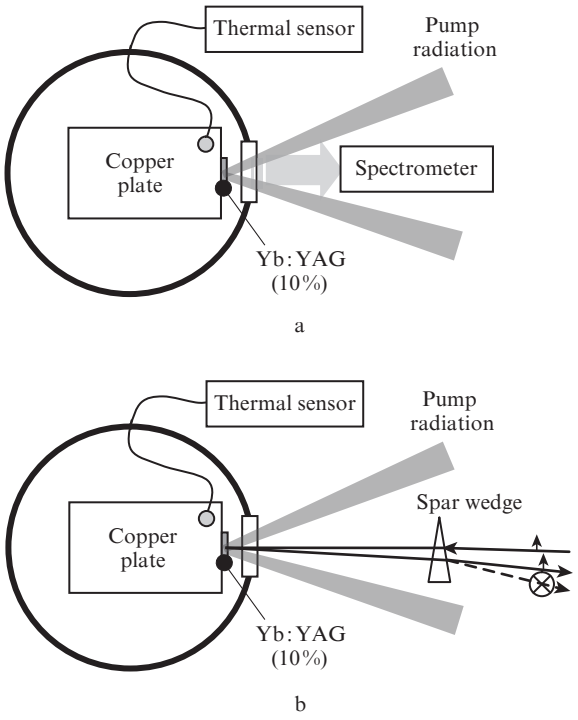


**Figure 1.** Setups for recording the luminescence spectrum (a) and the thermoinduced depolarisation (b) in a thin Yb:YAG crystal disk at different temperatures.

the crystal, and the amplified spontaneous emission could therefore be neglected. The luminescence spectrum was measured with a spectrometer at wavelength increments of 0.3 nm. To correctly measure the amplification cross section, one must make sure that the absorption of luminescence at this wavelength is negligible in the specimen under investigation. That is the reason why advantage was taken of a specimen of thickness of only 0.3 mm. In this specimen, at room temperature the absorption factor for luminescence was below 5% at a wavelength close to 1030 nm. The amplification cross section $\sigma$ is directly proportional to the luminescence intensity $P_{sp}(\nu)$ and inversely proportional to the lifetime $\tau$:

$$\sigma \sim \frac{P_{sp}(\nu)}{\nu^3}\frac{1}{P_{abs}\tau}, \qquad (1)$$

where $\nu$ is the frequency of radiation. Therefore, to calculate the absolute value of the amplification cross section at different temperatures one has to know its room-temperature value and the temperature dependence of the lifetime. We took the room-temperature value of amplification cross section obtained by averaging over the data of Refs [4, 11, 13–16] ($2.14\times10^{-20}$ cm$^2$) and borrowed the temperature dependence of the lifetime from Ref. [4].

Figure 2 shows the luminescence spectrum of Yb ions as a function of temperature. One can see that the width of the $\lambda = 1030$ nm line becomes much narrower on cooling and its intensity rises. Furthermore, the line peak and the average wavelength of the luminescence band exhibit shifts. Figure 3a serves to illustrate the 5.3-fold growth of the amplification cross section $\sigma_{max}$ at the peak of the luminescence line on cooling the crystal from 293 to 80 K. Similar measurements carried out in Ref. [4] showed a 4.3-fold increase in $\sigma_{max}$ and those of Ref. [11] displayed a 7-fold increase.

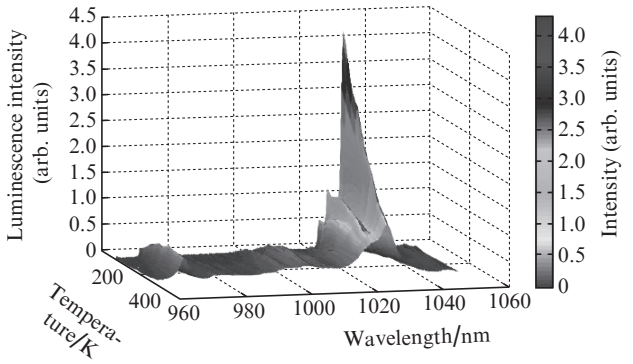


**Figure 2.** Wavelength and temperature dependences of the luminescence intensity of Yb ions in an Yb:YAG crystal doped with Yb ions with a density of 10%.

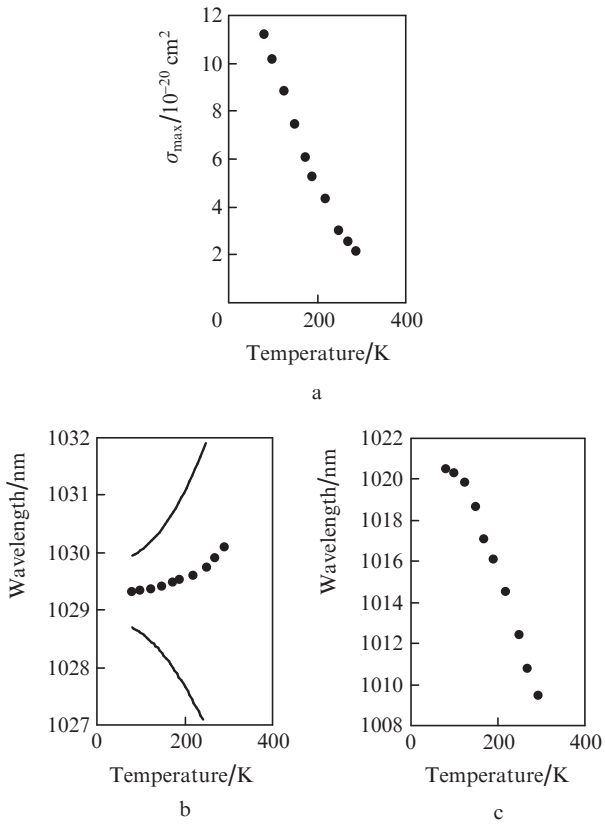


**Figure 3.** Temperature dependences of the peak amplification cross section (a), its corresponding wavelength $\lambda_{max}$ (b), and the luminescence centre-of-mass wavelength $\lambda_{mean}$ (c). The solid lines in Fig. 3b indicate the wavelengths at which the amplification cross section is equal to half the peak value.

Figure 3b depicts the temperature dependence of the wavelength $\lambda_{max}$ corresponding to the peak of amplification cross section. One can see that $\lambda_{max}$ shifts to the short-wavelength side by $\sim$0.8 nm on lowering the temperature. It is pertinent to note that the variation of $\lambda_{max}$ by $\sim$1 nm has received mention in Ref. [4]. At a temperature of 80 K the width of the luminescence spectrum is comparable to the $\lambda_{max}$ shift, so that a 1029.3-nm radiation source is required for obtaining efficient amplification. At room temperature, the lasing wavelength in Yb:YAG crystals exceeds 1030 nm. That is why operating a cryogenic Yb:YAG amplifier requires that either

the room-temperature Yb:YAG oscillator wavelength is artificially shifted or the Yb:YAG oscillator crystal is cooled.

The centre-of-mass amplification spectrum wavelength $\lambda_{mean}$ is another important characteristic of the amplification spectrum. The quantum defect in the medium and hence the heat liberation power in an Yb:YAG crystal depend on it. This problem will be considered in greater detail below. The $\lambda_{mean}$ wavelength, unlike $\lambda_{max}$, shifts to the long-wavelength side (from 1009 to 1020.5 nm) on cooling (Fig. 3c).

## 3. Thermal characteristics

The thermoinduced depolarisation $\gamma$ (the ratio between the power of depolarised part of radiation and its total power) and the 'thermal' lens are important characteristics of the active elements of high-power lasers. In this case, both the depolarisation and the lens parameters depend on the crystal orientation [17, 18] and are defined by the phase incursion $\delta_{1,2}$ in the two eigenpolarisations of thermoinduced birefringence and the angle $\Psi$ of eigenpolarisations inclination relative to one of crystallographic axes. For an active element in the form of a long cylinder, expressions for $\delta_{1,2}$ and $\psi$ for an arbitrary crystal orientation may be found in [19–22]. For the [001] and [111] orientations employed most frequently, these expressions were earlier derived in Refs [18, 23–27] and, correct to a non-essential constant, are of the form

$$\delta_{1,2} = kLP_{[001]}T(r) \pm kLQ\sqrt{\frac{1+\xi^2\tan^2(2\varphi-2\Phi)}{1+\tan^2(2\varphi-2\Phi)}}\left(\frac{1}{r^2}\int_0^r r^2\frac{\mathrm{d}T}{\mathrm{d}r}\mathrm{d}r\right),$$

$$\tan 2\Psi = \xi\tan 2\varphi \text{ for the [001] orientation,} \qquad (2)$$

$$\delta_{1,2} = kLP_{[111]}T(r) \pm kLQ\frac{1+2\xi}{3}\left(\frac{1}{r^2}\int_0^r r^2\frac{\mathrm{d}T}{\mathrm{d}r}\mathrm{d}r\right),$$

$$\Psi = \varphi \text{ for the [111] orientation,} \qquad (3)$$

where

$$Q = a_T\frac{n^3}{4}\frac{1+\sigma}{1-\sigma}(p_{11}-p_{12});$$

$$P_{[001]} = \frac{\mathrm{d}n}{\mathrm{d}T} - a_T\frac{n^3}{4}(1+\sigma)(p_{11}+p_{12});$$

$$P_{[111]} = P_{[001]} - \frac{\xi-1}{3}Q;\quad \xi = \frac{2p_{44}}{p_{11}-p_{12}};$$

$r$, $\varphi$ are cylindrical coordinates; $\Phi$ is the angle of rotation of the crystal about its geometrical axis; $k = 2\pi/\lambda$ is the wavenumber of the radiation transmitted through the crystal; $a_T$ is linear expansion coefficient; $n$ is the refractive index of the crystal; $\sigma$ is the Poisson coefficient; $p_{ij}$ are the elements of the photoelastic constant tensor of the medium; $L$ is the cylinder length; and $T$ is the crystal temperature. The quantities $P$ and $Q$ are referred to as thermooptical constants of the medium [19] and the quantity $\xi$ is termed the parameter of photoelastic anisotropy. As is evident from expressions (2) and (3), the constant $P$ characterises the optical strength of the thermal lens, $Q$ characterises the birefringence, and their ratio characterises the astigmatism of the thermal lens [18].

As follows from Ref. [28], similar formulas also apply to an active element in the form of a disk. For plane-stress disk deformations, formulas (2) and (3) are of the same form, with $Q$ replaced by the quantity $Q_{disk} = Q(1-\sigma)$.

The radial temperature gradient in an active element is proportional to the quantity $P_h/(\varkappa L)$ [18], where $P_h$ is the power of heat released in the crystal and $\varkappa$ is the thermal conductivity coefficient of the crystal. In view of expressions (2) and (3) we conclude: to determine the thermoinduced depolarisation $\gamma$ and the thermal lens parameters, one has to know five key parameters of the active element, specifically, $P_h$, $\varkappa$, $P$, $Q$ and $\xi$. The results of measurements of the temperature dependences of these quantities for an Yb:YAG crystal are given below.

### 3.1. Heat release

To calculate the thermoinduced distortions in an active element requires determining the heat power $P_h$ released in it. The fraction of pump power $P_{pump}$ deposited in the form of heat in the crystal, $\eta_h = P_h/P_{pump}$, may be described by the following expression [2]:

$$\eta_h = 1 - \eta_p\left[(1-\eta)\eta_r\frac{\lambda_p}{\lambda_{mean}} + \eta_{las}\frac{\lambda_p}{\lambda_{las}}\right], \qquad (4)$$

where $\eta_p$ is the efficiency of pump absorption; $\eta_r$ is the efficiency of emission from the upper metastable level; $\eta_{las}$ is the fraction of inversion which makes a contribution to laser radiation; $\lambda_p$ and $\lambda_{las}$ are the pump and laser radiation wavelengths. We consider an ideal case, whereby the pump radiation is completely absorbed ($\eta_p = 1$), there exist only radiative transitions from the upper metastable level ($\eta_r = 1$), and there is no laser radiation. In this case, the amount of heat released in the crystal is determined by the value of $\lambda_{mean}$. One can see from Fig. 3c that $\lambda_{mean}$ increases as the temperature is lowered. Consequently, $\eta_h$ will also increase and, under pumping at $\lambda_p = 940$ nm, will be equal to 6.8% at room temperature and to 7.9% at liquid nitrogen temperature. Therefore, one would expect a ~15% growth of heat deposition on cooling to 77 K. When the number of induced transitions is far greater than the number of spontaneous ones, the heat release in the crystal is defined by the quantum defect of $\lambda_p/\lambda_{las}$ and is equal to 8.7% at any crystal temperature.

We determined $\eta_h$ by measuring the thermoinduced polarisation distortions in the crystal under investigation [29]. The measurement setup is schematically shown in Fig. 1b. A 0.6-mm thick 10-mm long crystal of [001] orientation was placed in a copper bushing, which served as a heat sink. A beam of pump radiation with a known intensity profile was incident on the crystal. The probing radiation and the pump radiation with known intensity profiles were twice transmitted through the crystal. An optical wedge of feldspar (a spar wedge) extracted the depolarised component of the probing radiation. The pump power did not exceed 8 W, which ruled out a strong crystal heating.

The depolarisation was theoretically calculated using the programme code described in Ref. [30]. Knowing the thermooptical constant $Q$ ($5\times10^{-7}$ K$^{-1}$ [6, 8, 18]) and the thermal conductivity coefficient $\varkappa$, we selected $\eta_h$ such that the calculated data agreed with the experimental ones. In the specimen under investigation $\eta_h = 6.5\%$, which is close to the theoretical value (6.8%). The accuracy of this technique of measuring the heat release is rather high (the uncertainty is lower than 5% [29]),

but it depends on the accuracy of determining $\varkappa$. The calculation of heat release was carried out for the thermal conductivity coefficient measured for our crystals (see below). For a temperature of 77 K the quantity $\eta_h$ was not measured. In the subsequent discussion it is assumed that it increases to 7.6% according to Eqn (4) and Fig. 3c.

### 3.2. Thermal conduction

The thermal conductivity coefficient is an important characteristic of any active medium of a high-power laser. The effect of doping on the thermal conductivity of an Yb : YAG crystal was investigated in Refs [7, 14, 31]. We managed to find several papers [7, 31, 32] which reported measurements of the temperature dependence of the thermal conductivity coefficient for this crystal. By analysing these data it is possible to select a formula for calculating $\varkappa$ as a function of temperature and doping level which provides a satisfactory description of the data of these papers (Fig. 4):

$$\varkappa(T, C_{Yb}) = AT + B(C_{Yb})T^{-1} + C(C_{Yb})T^{-2}, \qquad (5)$$

where $A = 0.006$ W m$^{-1}$ K$^{-2}$; $B(C_{Yb}) = 1400^{-10} C_{Yb}$; $C(C_{Yb}) = 9\times10^5/(2 + C_{Yb})$ [$B(C_{Yb})$ is measured in W m$^{-1}$ and $C(C_{Yb})$ in W m$^{-1}$ K]; $C_{Yb}$ is the doping level in atomic percent. Formula (5) describes experimental data quite well for 80 K < $T$ < 350 K and 0 < $C_{Yb}$ < 30%. The thermal conductivity coefficient $\varkappa$ of an ionic crystal at low temperatures is determined by the mean free path of an acoustic phonon in the medium [33], i.e., depends on the amounts of impurities and the quality of the crystal lattice, which is affected by the method of crystal growth. In particular, for a TGG crystal grown from a melt, no temperature dependence of $\varkappa$ is observed in the 80–300 K range. Meanwhile, for a crystal grown from a solution, $\varkappa$ increases by a factor of two [33]. One can see from Fig. 4 that the thermal conductivity coefficient of Yb : YAG crystals becomes significantly lower with increase in doping level, and this effect is more pronounced at cryogenic temperatures.

We also measured the thermal conductivity coefficient of the crystals under investigation as a function of temperature. The data measured for $T$ = 300 K are close to the results of calculation by formula (5) ($\varkappa = 5 \pm 1.5$ W m$^{-1}$ K$^{-1}$). At the same time, only a minor increase in $\varkappa$ was observed on cooling. In the subsequent discussion it will be assumed that the thermal conductivity coefficient, which was measured with an uncertainty of ±20% for our specimens, is temperature-independent in the 80–300 K range. This may be attributed to the presence of a large amount of impurities, initial phase fragments in the specimens, and a poor quality of the crystal lattice.

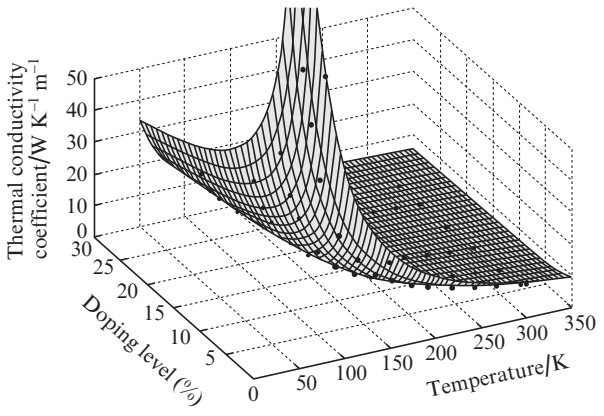


**Figure 4.** Experimental dependence [10, 19, 36] (points) and dependence calculated by formula (5) as functions of Yb : YAG crystal temperature and doping level.

### 3.3. Thermooptical constants $Q$ and $P$, parameter $\xi$

To measure the dependences of the thermooptical constant $Q$ and the photoelastic anisotropy parameter $\xi$, advantage was taken of the methods of Refs [19, 34]. Measurements were made of depolarisation in an [001]-oriented Yb : YAG crystal doped with Yb ions to a density of 10%. In this case, the depolarisation depends on the angle between one of crystallographic axes and the direction of polarisation of the probing radiation. By rotating the crystal about its geometrical axis (by varying the $\Phi$ angle) it is possible to obtain the maximal ($\gamma^{max}_{[001]}$) or minimal ($\gamma^{min}_{[001]}$) depolarisation, with $\gamma^{max}_{[001]}/\gamma^{min}_{[001]} = \xi^2$ [24].

The technique of measuring depolarisation is described in the foregoing. We only note that the direction of polarisation of the probing radiation for attaining the minimum and maximum of depolarisation was varied with the aid of a $\lambda/2$ plate placed between the crystal and the spar wedge. The pump power at which these measurements were made did not exceed 10 W, and its wavelength was so selected (~938 nm) that the absorption of the pumping radiation was temperature-independent. The heat was removed via the side surface of the disk, because the thermoinduced depolarisation was too small when the heat was removed via the disk face. According to Fig. 3c and formula (4), the heat release rises by 15% on cooling the crystal to 77%, which was included in our calculations. It is also noted that in our experiment the crystal could be heated above the temperature indicated by the thermal sensor. To estimate this heating, we recorded variations of the luminescence spectrum throughout the experiment. By using the dependence shown in Fig. 3a as a calibration one, we estimated the average crystal temperature in the region of pump absorption. Our measurements showed that the crystal temperature exceeded the readings of the thermal sensor by about 40 ± 5 K throughout the measurement range (80–300 K).

Figure 5a shows the crystal-temperature dependences of the thermoinduced depolarisation corresponding to the maximum ($\gamma^{max}_{[001]}$) and minimum ($\gamma^{min}_{[001]}$) of depolarisation. With the knowledge of heat deposition in the crystal and the temperature dependence of the thermal conductivity coefficient, by formulas (2) and (3) it is easy to calculate the thermooptical constant $Q$ and the photoelastic anisotropy parameter $\xi$ (Figs 5b and c).

With reference to Fig. 5d, the measured dependence $Q(T)$ coincides with the temperature dependence of the linear expansion coefficient. In view of the fact that the Poisson coefficient and the refractive index are only slightly dependent on the temperature, the difference $p_{11} - p_{12}$ may be assumed to be temperature-independent [see formulas (2) and (3)]. In this case, the variation of $\xi$ takes place due to the variation of $p_{44}$. Furthermore, since $p_{11}$ in an YAG crystal is 10 times greater than $p_{12}$, it is reasonable to assume that the sum $p_{11} + p_{12}$ does not change significantly in the 80–300 K temperature range. Then, invoking the temperature dependences of d$n$/d$T$ and $a_T$ from Ref. [6], it is possible to construct the temperature dependences of the parameter $P$ (Fig. 6). As is evident from Fig. 6, on cooling the crystal, first, the parameter $P$ (and hence

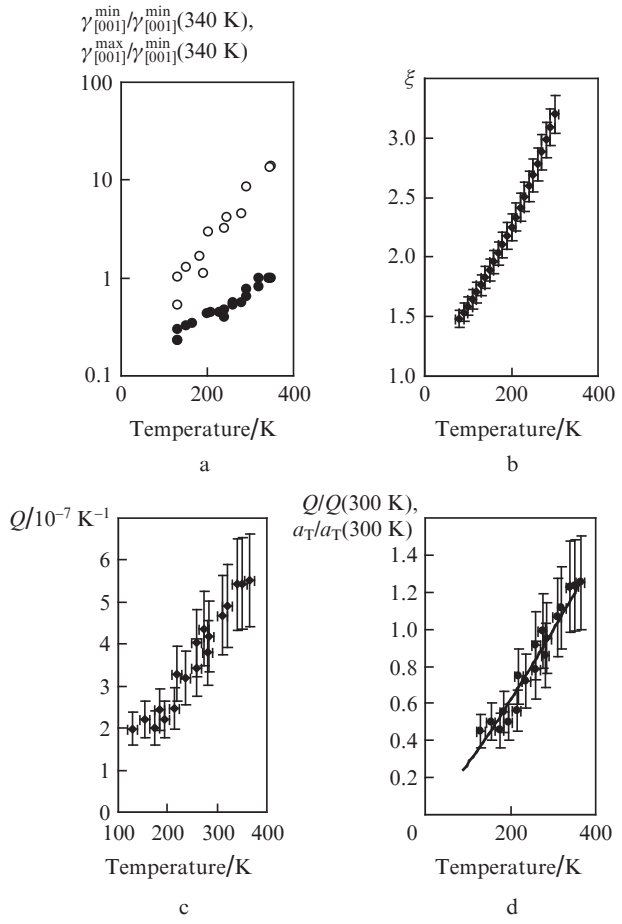


**Figure 5.** Temperature dependences of the normalised depolarisations $\gamma^{max}_{[001]}/\gamma^{min}_{[001]}$(340 K) (○) and $\gamma^{min}_{[001]}/\gamma^{min}_{[001]}$(340 K) (●) (a), the photoelastic anisotropy parameter $\xi$ (b), the thermooptical constant $Q$ (c), as well as the normalised linear expansion coefficient $a_T$ [9] (solid curve) and the normalised thermooptical constant $Q$ (points) (d).

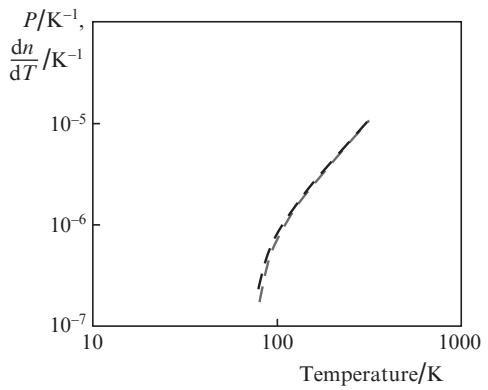


**Figure 6.** Thermooptical constants $P$ (grey curve) and d$n$/d$T$ (black curve) as functions of the temperature.

the focal power of the thermal lens) becomes significantly smaller and, second, the contribution from the photoelastic effect becomes comparable to the contribution from the temperature dependence of the refractive index. In addition, for $T < 300$ K the values of $P$ and $Q$ turn out to be comparable, which implies a strong astigmatism of the thermal lens.

To calculate phase distortions in the general case requires also taking into account the effect of population inversion in the medium on the refractive index (the so-called electronic lens) [35]. At room temperature this effect may be neglected when the pump power density is much lower than the saturation power density, which is usually the case for lasers with a high average output power. When 17% of the total number of the doping ions are inverted in the 600-μm thick Yb:YAG crystal with a 6-mm diameter of the domain with population inversion, the focal length of the electronic lens is equal to 450 m [29]. This distance is far greater than the focal length of the thermal lens in the crystal under continuous pumping even at cryogenic temperatures [29]. On the other hand, the electronic lensing may turn out to be the governing effect under pulsed pumping at a low pulse repetition rate [36].

## 4. Conclusions

In this work we give all dependences of material constants of an Yb:YAG crystal required for calculating the amplification parameters as well as polarisation and phase distortions of radiation. A part of the data was obtained for the first time, another part was defined more precisely or repeated and is in good agreement with the data of other papers. Lowering the Yb:YAG crystal temperature does improve the lasing and thermal characteristics of the crystal. The amplification cross section increases and becomes comparable to that of the Nd:YAG crystal, and the amplification linewidth narrows to 1.3 nm, which is sufficient for the amplification of a picosecond pulse. The peak of the amplification cross section shifts to the short-wavelength side, which must be taken into consideration in the amplification of signals in cryogenic amplifiers. Furthermore, the quantum defect of an Yb:YAG crystal laser increases on cooling, which may result in an increase of heat deposition in the active element. An increase in thermal conductivity coefficient and a decrease in thermooptical constants $P$ and $Q$ make it possible to make substantially heavier the thermal load on the active element. A lowering in thermooptical anisotropy parameter weakens the dependence of polarisation distortions on crystal orientation. At temperatures close to 80 K, the quantities $Q$ and $P$ become comparable, resulting in an increase of the astigmatism of the thermal lens.

***Acknowledgements.*** The authors express their appreciation to I.A. Ivanov and A.M. Bul'kanov for the given specimens.

This work was supported by the 'Extreme Light Fields: Sources and Applications' Programme of the Presidium of the Russian Academy of Sciences and the Russian Foundation for Basic Research (Grant No. 08-02-99044-p_ofi).

## References

1. Krupke W. *IEEE J. Sel. Top. Quantum Electron.*, **6**, 1287 (2000).
2. Fan T.Y. *IEEE J. Quantum Electron.*, **29**, 1457 (1993).
3. Giesen A., Hugel H., Voss A., Wittig K., Brauch U., Opower H. *J. Appl. Phys. B*, **58**, 365 (1994).
4. Dong J., Bass M., Mao Y., Gan P.D.F. *J. Opt. Soc. Am. B*, **20**, 1975 (2003).
5. Brown D.C., Cone R.L., Sun Y., Equall R.W. *IEEE J. Sel. Top. Quantum Electron.*, **11**, 604 (2005).
6. Fan T.Y., Daneu J.L. *Appl. Opt.*, **37**, 1635 (1998).
7. Bourdet G.L., Yu H. *Appl. Opt.*, **46**, 6033 (2007).
8. Brown D.C. *IEEE J. Quantum Electron.*, **34**, 2383 (1998).
9. Fan T.Y., Crow T., Hoden B. *Proc. SPIE Int. Soc. Opt. Eng.*, **3381**, 200 (1998).
10. Brown D.C. US Patent 6195372 (2001).

11. Tokita S., Kawanaka J., Fujita M., Kawashima T., Izawa Y. *Appl. Phys. B*, **80**, 635 (2005).
12. Ripin D.J., Ochoa J.R., Agarwal R.L., Fan T.Y. *Opt. Lett.*, **29**, 2154 (2004).
13. Bruesselbach H.W., Sumida D.S., Reeder R.A., Byren R.W. *IEEE J. Sel. Top. Quantum Electron.*, **3**, 105 (1997).
14. Patel F.D., Honea E.C., Speth J., Payne S.A., Hutcheson R., Equall R. *IEEE J. Quantum Electron.*, **37**, 135 (2001).
15. Casagrande O., Deguil-Robin N., Garrec B.L., Bourdet G.L. *IEEE J. Quantum Electron.*, **43**, 206 (2007).
16. He X., Zhao G., Xu X., Zeng X., Xu J. *Chin. Opt. Lett.*, **5**, 295 (2007).
17. Mukhin I.B., Palashov O.V., Khazanov E.A., Ivanov I.A. *Pis'ma Zh. Eksp. Teor. Fiz*., **81**, 120 (2005).
18. Mezenov A.V., Soms L.N., Stepanov A.I. *Termooptika tverdotel'nykh lazerov* (Thermooptics of Solid State Lasers) (Leningrad: Mashinostroenie, 1986).
19. Khazanov E., Andreev N., Palashov O., Poteomkin A., Sergeev A., Mehl O., Reitze D. *Appl. Opt.*, **41**, 483 (2002).
20. Snetkov I.L., Mukhin I.B., Palashov O.V., Khazanov E.A. *Kvantovaya Elektron*., **37**, 633 (2007) [*Quantum Elektron*., **37**, 633 (2007)].
21. Mukhin I.B., Palashov O.V., Snetkov I.L., Khazanov E.A. *Proc. SPIE Int. Soc. Opt. Eng.*, **6610**, 66100N (2007).
22. Mukhin I.B., Palashov O.V., Khazanov E.A. *Proc. SPIE Int. Soc. Opt. Eng*., **5975**, 59750G (2006).
23. Soms L.N., Tarasov A.A., Shashkin V.V. *Kvantovaya Elektron.*, **7**, 619 (1980) [*Sov. J. Quantum Elektron*., **10**, 350 (1980)].
24. Massey G.A. *Appl. Phys. Lett.*, **17**, 213 (1970).
25. Foster J.D., Osterink L.M. *J. Appl. Phys.*, **41**, 3656 (1970).
26. Koechner W. *Appl. Opt.*, **9**, 1429 (1970).
27. Koechner W., Rice D.K. *IEEE J. Quantum Electron.*, **6**, 557 (1970).
28. Mit'kin V.M., Shchavelev O.S. *Opt.-Mekh. Prom*., **9**, 26 (1973).
29. Palashov O.V., Khazanov E.A., Mukhin I.B., Smirnov A.N., Mironov I.A., Dukel'skii K.V., Garibin E.A. *Kvantovaya Elektron*., **39**, 943 (2009) [*Quantum Elektron*., **39**, 943 (2009)].
30. Vyatkin A.G., Khazanov E.A. *Kvantovaya Elektron*., **39**, 814 (2009) [*Quantum Elektron*., **39**, 814 (2009)].
31. Tokita S., Kawanaka J., Izawa Y., Fujita M., Kawashima T. *Techn. Dig. Conf. 'Advanced Solid-State Photonics'* (Incline Village, Nevada, USA, 2006) TuB16.
32. Wang B., Jiang H., Jia X., Zhang Q., Sun D., Yin S. *Front. Optoelectron. China*, **1** (1-2), 138 (2008).
33. Slack G.A., Oliver D.W. *Phys. Rev. B*, **4**, 592 (1971).
34. Khazanov E., Andreev N., Palashov O., Poteomkin A., Sergeev A., Mehl O., Reitze D. *Appl. Opt.*, **41**, 483 (2002).
35. Antipov O.L., Eremeikin O.N., Savikin A.P. *Kvantovaya Elektron*., **33**, 861 (2003) [*Quantum Elektron*., **33**, 861 (2003)].
36. Antipov O.L., Anashkina E.A., Fedorova K.A. *Kvantovaya Elektron*., **39**, 1131 (2009) [*Quantum Elektron*., **39**, 1131 (2009)].